ICAS 2016
30th Congress of the International Council of the Aeronautical Sciences
DCC, Daejeon, Korea ; September 25-30, 2016

NONLINEAR DYNAMIC INVERSION WITH NEURAL NETWORKS FOR THE FLIGHT CONTROL OF A LOW COST TILT ROTOR UAV

Egidio D'Amato*, Gaetano Tartaglione, Luciano Blasi*, Massimiliano Mattei***
***Dipartimento di Ingegneria Industriale e dell'Informazione, Seconda Università degli Studi di Napoli**
****Dipartimento di Ingegneria, Università degli Studi di Napoli "Parthenope"**

Keywords: *nonlinear dynamic inversion; neuro-adaptive compensation, tilt rotor unmanned aerial vehicle; real time embedded control*

Abstract

This paper deals with the development of a flight control scheme based on the Nonlinear Dynamic Inversion technique (NDI). Such a scheme has been implemented on the Flight Control System (FCS) of a trirotors prototype model used to simulate tilt rotor air vehicles dynamics during all those phases when aerodynamic surfaces are less effective or not effective at all. An adaptive flight control scheme has been developed based on Radial Basis Function Neural Network (RBFNN) and NDI making both attitude and trajectory tracking control system less sensitive to modelling errors. To demonstrate the effectiveness of the proposed control technique both numerical simulations and experimental tests have been performed. To this end a scaled multi-rotor test bed has been built simulating a tilt rotor unmanned air vehicle (UAV) in hovering and low speed flight conditions. The control system has been implemented on an embedded board based on an ARM Cortex M4 processor and a low cost Inertial Measurement Unit with triaxial MEMS accelerometer, gyroscope and magnetometer sensors. As accuracy of NDI control system can be affected by model uncertainties and sharp transients due to the RBFNN adaptation transients, a model calibration phase is needed. To this end preliminary flight tests have been performed for UAV dynamic model identification and control parameters tuning.

1 Introduction

Innovative aerial vehicles have proved themselves in different areas of military and civil applications over a hundred years, by enhancing their capabilities over time, and adapting to new mission requirements.

Different capabilities like Vertical Take-Off and Landing (VTOL), hover, level flight, mode switching between hover and level modes, high endurance, long range and mechanical simplicity are expected from unmanned air vehicle (UAV) platforms according to mission requirements. When VTOL and hovering capabilities are required, then rotary-wing aircraft such as helicopters, multirotors, ducted fans, tiltrotors and tailsitters are the optimal choice.

On the other hand, if level flight, endurance or range performance are a top priority, then a fixed-wing airplane type will most likely be preferred due to its higher efficiency. When all of these features are desired, then VTOL-FW (VTOL-Fixed Wing) platform becomes the best option. VTOL capability removes the need for runway or launch/recovery equipment and provides flexibility to operate in any theatre, whereas level flight capability allows quite satisfactory performance in terms of range and endurance. An aerial vehicle designed to possess the strengths of both rotary and fixed-wing aircraft will have both the advantages in one platform,

with acceptable trade-offs in some capabilities [1].

Tiltrotor configurations have been the most successful and widely applied high speed VTOL air vehicle design solution. After being shown to be technically feasible with the McDonnell XV-3 and the Bell XV-15 [2], the tiltrotor concept has now seen many thousands of hours of successful operation following the introduction of the V-22 into service in 2007. Pending further prototype flight testing, the AgustaWestland 609 is projected to extend these capabilities into the civil field starting in 2018 [3].

Design of a Flight Control Systems (FCSs) for this kind of UAVs can be very difficult due to their nonlinear dynamic response, the transition phase between hovering and forward flight and the large cross coupling effects. Hovering and forward flight typically need a separate control strategy: during hovering, only thrust vectoring can be used to control the aircraft acting as a multi rotor with tilting propellers, whereas during forward flight classical aerodynamic surfaces can be also used. During transition phase tilt rotors need a blending strategy, defining the control effort allocation among the available effectors.

Several approaches have been proposed in the literature for the flight control of small scale tilt rotors UAVs. Most of them have been tested by numerical simulations with few flying platforms [4, 5, 6, 7, 8, 9, 10, 11, 12].

One of the most promising and popular nonlinear techniques for flight control applications is the Nonlinear Dynamic Inversion (NDI), already used for several multi-rotor hovering aircrafts. NDI is a control technique which attempts to cancel out the inherent dynamics of a plant enforcing dynamics of a reference model. The most important benefits of NDI technique are its ability to linearize systems, decouple controlled variables, separate reference model from dynamic inversion model and compute solution in a closed form. However, NDI exhibits strong sensitivity to modelling errors and external disturbances. To reduce this sensitivity and solve the lack of control affinity problem, the technique can be improved using the Incremental NDI (INDI) [13, 14]. To face with this problem, also adaptive control is used in combination with NDI. In particular, Neural Network-based adaptive aircraft control has been extensively studied with different strategies [15, 16, 17, 18, 19].

In this paper, an adaptive flight control technique based on Radial Basis Function Neural Network (RBFNN) and NDI is adopted to design attitude and trajectory tracking control actions for tilt rotor UAVs. This method can guarantee the convergence of tracking error also in the presence of modelling errors.

To test the effectiveness of the proposed control techniques during hovering and low speed flight phases a tilt-tri-rotor small scale UAV has been designed and built (Fig. 1).

Fig. 1 – Tilt-trirotor flying platform

The developed tilt-trirotor represents a novel configuration in the mini-UAV panorama, due to the front tilting rotors used for yaw control and for level flight. In literature the most known trirotors have the rear tilting rotor to control the yaw attitude [20, 21] or all tilting rotors [22]. Differently, the configuration shown in this paper is able to perform level flight with negligible attitude change thanks to the front tilting rotors. This capability represents a very interesting feature both for photographic purposes, as it avoids the installation of too complex and heavy gimbal systems (relatively to micro UAV), and for a more effective control of a tilt rotor UAV with aerodynamic surfaces during the transition phase between hovering and forward flight.

2 Tri-rotor dynamic model

The nonlinear mathematical model of UAVs can be easily obtained from the standard nonlinear 6DoF (Degree of Freedom) rigid aircraft model. The system motion can be described adopting two reference frames: an inertial earth-fixed frame, E, and a body-fixed frame, B, whose origin O_B is located in the vehicle CoG (Center of Gravity). Vehicle position in the earth-fixed frame E is defined as $\boldsymbol{\zeta} = [x_E, y_E, z_E]^T$ whereas its orientation is denoted as $\boldsymbol{\Theta} = [\phi, \vartheta, \psi]^T$ where $\phi, \vartheta,$ and ψ are the roll, pitch, and yaw angle respectively.

The dynamic model of rigid body UAV in the body-fixed frame B can be written as:

$$\begin{bmatrix}\dot{u}\\ \dot{v}\\ \dot{w}\end{bmatrix} = \frac{1}{m}\left(-\begin{bmatrix}p\\ q\\ r\end{bmatrix} \times \mathrm{m}\begin{bmatrix}u\\ v\\ w\end{bmatrix} + \boldsymbol{F}(V_B, \Omega, \Theta, \zeta, \bar{\omega}, \gamma)\right) \quad (1)$$

$$\begin{bmatrix}\dot{p}\\ \dot{q}\\ \dot{r}\end{bmatrix} = \boldsymbol{I}^{-1}\left(-\begin{bmatrix}p\\ q\\ r\end{bmatrix} \times I\begin{bmatrix}p\\ q\\ r\end{bmatrix} + \boldsymbol{T}(V_B, \Omega, \zeta, \bar{\omega}, \gamma)\right) \quad (2)$$

where m is the aircraft mass, $\boldsymbol{I}$ is the inertia matrix, $\boldsymbol{V}_B = [u, v, w]^T$ and $\boldsymbol{\Omega} = [p, q, r]^T$ are the velocity and angular velocity vector in the frame B respectively.

The attitude dynamics can be expressed as a function of $\boldsymbol{\Omega}$ as:

$$\begin{bmatrix}\dot{\phi}\\ \dot{\theta}\\ \dot{\psi}\end{bmatrix} = \begin{bmatrix}1 & sin\phi \cdot tan\theta & cos\phi \cdot tan\theta\\ 0 & cos\phi & -sin\phi\\ 0 & \frac{sin\phi}{cos\theta} & \frac{cos\phi}{cos\theta}\end{bmatrix}\begin{bmatrix}p\\ q\\ r\end{bmatrix} \quad (3)$$

In order to obtain the inertial position, it also can be written that:

$$\begin{bmatrix}\dot{x_E}\\ \dot{y}_\mathrm{E}\\ \dot{z}_\mathrm{E}\end{bmatrix} = \boldsymbol{R}_{BE}^{-1}(\phi, \theta, \psi)\begin{bmatrix}u\\ v\\ w\end{bmatrix} \quad (4)$$

where $\boldsymbol{R}_{BE}$ is the rotation matrix from the earth-fixed reference frame to body axis.

The external forces and moments in (1) and (2) depend on $\boldsymbol{V}_B$, $\boldsymbol{\Omega}$, $\boldsymbol{\Theta}$, $\boldsymbol{\zeta}$, rotational speed of the propellers $\bar{\boldsymbol{\omega}} = [\omega_1, \omega_2, \omega_3]^T$, and tilting angles of the two front rotors $\boldsymbol{\gamma} = [\gamma_1, \gamma_2]^T$.

The force vector $\boldsymbol{F}$ and the moment vector $\boldsymbol{T}$ can be written as sum of different terms:

$$\boldsymbol{F} = \boldsymbol{F}_g + \boldsymbol{F}_p + \boldsymbol{F}_a \quad (5)$$

$$\boldsymbol{T} = \boldsymbol{T}_p + \boldsymbol{T}_a \quad (6)$$

where $\boldsymbol{F}_g$ is the gravitational force, $\boldsymbol{F}_p$ and $\boldsymbol{T}_p$ are propulsive forces and moments, $\boldsymbol{F}_a$ and $\boldsymbol{T}_a$ are aerodynamic forces and moments. The gravitational force $\boldsymbol{F}_g$ is:

$$\boldsymbol{F}_g = mg[sin\theta \quad -sin\phi \quad -cos\theta cos\phi]^T \quad (7)$$

In near hover conditions, propeller forces $\boldsymbol{F}_p$ and moments $\boldsymbol{T}_p$ are nonlinear functions of rotors speed and tilting angles γ_1 and γ_2. To achieve a partial decoupling these angles can be written as the sum of a symmetric command α and a non-symmetric command β:

$$\gamma_1 = \alpha + \beta \quad (8)$$

$$\gamma_2 = \alpha - \beta \quad (9)$$

The propulsive force and moment, $\boldsymbol{F}_p$ and $\boldsymbol{T}_p$ respectively, are defined as follows:

$$\boldsymbol{F}_p = [F_x \;\; 0 \;\; F_z]^T \quad (10)$$

$$\boldsymbol{T}_p = [L \; M \; N]^T \quad (11)$$

where F_x, F_z, L, M, N are related to aerodynamic forces and moments of propellers F_i and T_i, i=1,2,3. We assume that F_i and T_i depend on the i-th rotor speed ω_i as:

$$F_i = k_f\omega_i^2 \quad (12)$$

$$T_i = k_t\omega_i^2 \quad (13)$$

where k_f and k_t are the propeller force and torque coefficients, respectively. Then forces F_x, F_z and moments L, M, N are calculated as follows:

$$\begin{bmatrix}F_x\\ F_z\\ L\\ M\\ N\end{bmatrix} = \bar{\boldsymbol{R}}\begin{bmatrix}k_f\omega_1^2\\ k_f\omega_2^2\\ k_f\omega_3^2\\ k_t\omega_1^2\\ k_t\omega_2^2\\ k_t\omega_3^2\end{bmatrix} \quad (14)$$

Matrix $\bar{\boldsymbol{R}}$ in (14) is defined as:

$$\bar{\boldsymbol{R}} = \begin{bmatrix}s\gamma_1 & s\gamma_2 & 0 & 0 & 0 & 0\\ c\gamma_1 & c\gamma_2 & 1 & 0 & 0 & 0\\ b\cdot c\gamma_1 & -b\cdot c\gamma_2 & 0 & s\gamma_1 & s\gamma_2 & 0\\ l_f\cdot c\gamma_1 & l_f\cdot c\gamma_2 & -l_r & 0 & 0 & 0\\ b\cdot s\gamma_1 & -b\cdot s\gamma_2 & 0 & c\gamma_1 & c\gamma_2 & 1\end{bmatrix} \quad (15)$$

where $s\gamma_i$ indicates $sin(\gamma_i)$, $c\gamma_i$ indicates $\cos(\gamma_i)$, b and l_f are the distance of front rotors from CG along y-axis and x-axis respectively, l_r is the distance of rear rotor from CG along x-

axis (Fig. 2). Tilt-trirotor main characteristics are reported in Table 1.

Table 1. Tilt-tri-rotor main characteristics.

Name	*Description*	*Value*
m	Mass	$1.5\ kg$
l_f	Distance of front props from CG along x axis	$0.104\ m$
l_r	Distance of rear prop from CG along x axis	$0.208\ m$
b	Distance of front props from CG along y axis	$0.180\ m$
I_{xx}	Moment of inertia about x axis	$23.08 \cdot 10^{-3} kgm^2$
I_{yy}	Moment of inertia about y axis	$27.38 \cdot 10^{-3} kgm^2$
I_{zz}	Moment of inertia about z axis	$46.72 \cdot 10^{-3} kgm^2$
τ_r	Time constant of rotor dynamics (nominal)	$0.01\ s$
k_f	Force coefficient (identified by wind tunnel tests)	$5 \cdot 10^{-2}\ Ns^2$
k_t	Torque coefficient (identified by wind tunnel tests)	$5 \cdot 10^{-4}\ Nms^2$
τ_s	Time constant of servo dynamics (nominal)	$0.01\ s$

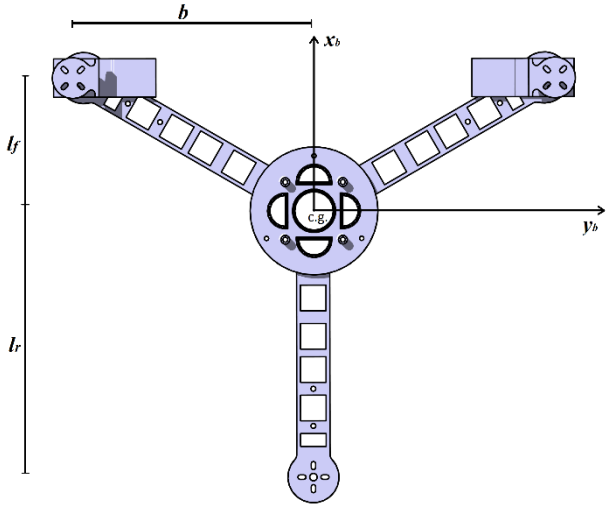

Fig. 2 - Rotor arms geometry

Owing to the low dynamic pressure in near hover conditions, the absence of lifting surfaces and the lack of experimental data at small Reynolds numbers, aerodynamic forces and moments are neglected. The state vector of model in eqns. (1-4) includes state variables and control inputs, namely $(\omega_1^2, \omega_2^2, \omega_3^2, \gamma_1, \gamma_2)$.

3 Flight Control Law

The tri-rotor vehicle can be controlled in a Remotely Piloted Vehicle (RPV) mode or in a Command Directed (CD) mode.

A hierarchical structure is adopted to separate tracking control and attitude control [23]. The overall flight control system is composed of three main parts (see Fig.3):

- a NDI outer loop (NDI Slowloop) controlling the slow dynamics and generating a state command to the inner block;
- a NDI inner loop (NDI Fastloop) controlling the fast dynamics and outputting virtual commands (requested forces and moments) to the effectors;
- a Control Allocator block distributing the control effort among the available effectors.

3.1 NDI Outer Loop Control

Trajectory commands are given in terms of waypoint positions (x_c, y_c, z_c) and reference heading angle ψ_c, at the outer level. The outer loop characteristic frequency is 5Hz.

Considering small pitch and roll angle, equations (1) and (4) are combined, and the external loop controller is designed assuming:

$$F_z = m(\ddot{z} + g) \qquad (16)$$

$$F_x = m(\ddot{x}\cos\psi + \ddot{y}\sin\psi) \qquad (17)$$

Assuming that $F_y \cong F_z\phi$, the control on y

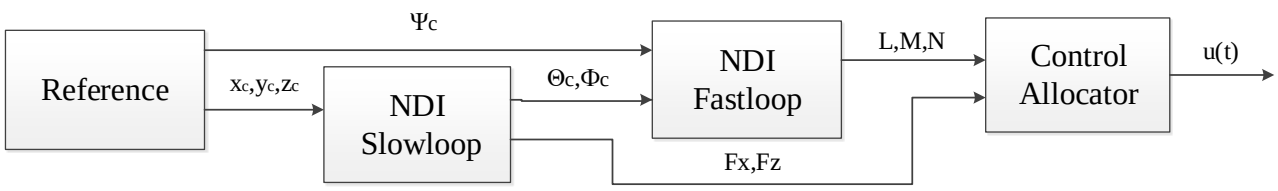

Fig. 3 - NDI control system architecture

axis can be performed through the roll command by using equation (18):

$$\phi_c = \frac{m}{F_z}(\ddot{x}\sin\psi - \ddot{y}\cos\psi) \tag{18}$$

If we consider a trajectory control that exponentially stabilizes the waypoint position error, then the desired acceleration command satisfies the following relationships:

$$F_z = m(-k_w\dot{z} - k_w k_z(z - z_c) + g) \tag{19}$$

$$\begin{aligned} F_x = {} & -m\cos\psi\left(-k_u\dot{x} - k_u k_x(x - x_c)\right) \\ & + +m\sin\psi\left(-k_y\dot{y}\right. \\ & \left. - k_v k_y(y - Y_c)\right) \end{aligned} \tag{20}$$

$$\begin{aligned} \phi_c = \frac{1}{g}\Big(&\sin\psi\left(-k_u\dot{x} - k_u k_x(x - x_c)\right) \\ &- \cos\psi\left(-k_y\dot{y} - k_v k_y(y - y_c)\right)\Big) \end{aligned} \tag{21}$$

where k_x, k_y, k_z and k_u, k_v, k_w are related to the damping factor ξ and natural frequency ω of the closed loop system, namely:

$$k_x = k_y = k_z = \frac{\omega}{2\xi} \tag{22}$$

$$k_u = k_v = k_w = 2\omega\xi \tag{23}$$

3.2 NDI Inner Loop Control

The inner loop controls attitude and has a characteristic frequency of about 100Hz.

Virtual commands are sent to the control allocator in terms of moments (L, M, N) computed as:

$$\begin{Bmatrix} L \\ M \\ N \end{Bmatrix} = \begin{bmatrix} I_{xx}k_p(p_c - p) \\ I_{yy}k_q(q_c - q) \\ I_{zz}k_r(r_c - r) \end{bmatrix} + \begin{bmatrix} (I_{zz} - I_{yy})qr \\ (I_{xx} - I_{zz})pr \\ (I_{yy} - I_{xx})pq \end{bmatrix} \tag{24}$$

where reference angular speeds (p_c, q_c, r_c) can be computed from eq. (3) on the basis of the reference pitch and roll angles (ϕ_c, θ_c) given by the outer loop as:

$$\begin{Bmatrix} p_c \\ q_c \\ r_c \end{Bmatrix} = \begin{bmatrix} 1 & \sin\phi\tan\theta & \cos\phi\tan\theta \\ 0 & \cos\phi & -\sin\phi \\ 0 & \frac{\sin\phi}{\cos\theta} & \frac{\cos\phi}{\cos\theta} \end{bmatrix}^{-1} \begin{Bmatrix} k_\phi(\phi_c - \phi) \\ k_\theta(\theta_c - \theta) \\ k_\psi(\psi_c - \psi) \end{Bmatrix} \tag{25}$$

Coupling terms in the right hand side of equation (24) are neglected to assure zero control commands (L=M=N=0), whenever velocity error is zero. All the non-modelled dynamics are then balanced using the adaptive scheme described in Section 4.

As for constants k_ϕ, k_θ, k_ψ and $k_p I_{xx}, k_q I_{yy}, k_r I_{zz}$, they can be computed with the same methodology previously used for the outer slow loop controller.

3.3 Control Allocator

Virtual commands given in terms of forces and moments must be translated in terms of real input commands to control rotors speed and tilt angles managing the effectors redundancy if needed. Control allocation can be computed from eqs. (8), (9), (14) and (15):

$$\begin{bmatrix} \omega_1^2 \\ \omega_2^2 \\ \omega_3^2 \\ \alpha \\ \beta \end{bmatrix} = \begin{bmatrix} 0 & \frac{1}{4} & \frac{1}{4l_r} & \frac{1}{4l_f} & 0 \\ 0 & \frac{1}{4} & -\frac{1}{2l_r} & \frac{1}{4l_f} & 0 \\ 0 & \frac{1}{2} & 0 & -\frac{1}{2l_r} & 0 \\ \frac{1}{2} & 0 & 0 & 0 & 0 \\ 0 & 0 & 0 & 0 & \frac{1}{2b} \end{bmatrix} \cdot \begin{bmatrix} \frac{F_x}{k_f} \\ \frac{F_z}{k_f} \\ \frac{L}{k_f} \\ \frac{M}{k_f} \\ \frac{N}{k_f} \end{bmatrix} \tag{26}$$

4 Neural Network Augmented Control

The strong sensitivity of NDI technique to dynamic model accuracy requires an adaptive approach that is able to compensate modelling errors in a real time manner.

Fig. 4 shows the control scheme including the Reference Model, the NDI and a NN-based adaptive compensator. The modelling error feeds the NN which generates, on the basis of the system input and state, an additive input to compensated deviations due to the approximate NDI. This approach is known in the literature as Approximate Model Inversion (AMI) Model Reference Adaptive Control (MRAC).

If the uncertainty structure is unknown, RBFNNs can be efficiently used. They are single hidden layer-type neural networks, with nonlinear hidden layer and linear output layer. The activation functions are RBFs, whose argument is the Euclidean norm between the input vector and a given center. The most popular RBFs are Gaussian functions:

$$\varphi(x) = e^{-\frac{\|x-\mu\|^2}{\sigma^2}} \quad (27)$$

where μ and σ are the radial basis function center end width respectively.

The universal approximation property states that given a sufficient number of radial basis functions, there exists a set of ideal weights such that the error ε can be made arbitrary small, where ε represents the difference between actual deviation of the approximate model from the true dynamics (real modeling error, d) and the NN ideal compensation (estimated modeling error with ideal weights, $\bar{d}$):

$$\varepsilon = d(\boldsymbol{z}) - \bar{d}(\boldsymbol{z}) \quad (28)$$

where $\boldsymbol{z}$ is the vector of parameters affecting the modeling error, which include state and control variables $(\boldsymbol{x}, \boldsymbol{u})$.

Pseudo control for the NDI can be written as (see Fig. 4):

$$\dot{y}_a = \dot{y}_{rm} + K_e e + \hat{d} \quad (29)$$

where $e = y_{rm} - y$ and $\hat{d}$ is the NN output (estimated modeling error with actual weights).

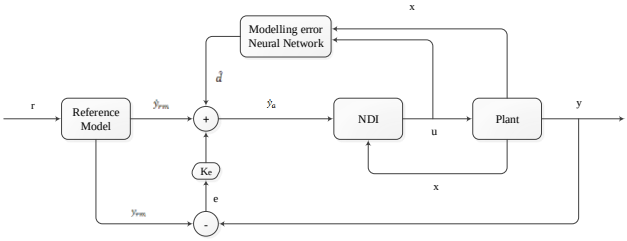

Fig. 4. Architecture of NN augmented NDI

having defined d as the modeling error:

$$d = \dot{y}_a - \dot{y} \quad (30)$$

The following error dynamics can be obtained combining equations (28), (29) and (30):

$$\dot{e} + K_e e + \hat{d} - \bar{d} - \varepsilon = 0 \quad (31)$$

The output of a NN can be expressed in matrix form:

$$\begin{aligned} \bar{d}(z) &= \overline{\boldsymbol{W}}^T \varphi(\boldsymbol{z}) \\ \hat{d}(z) &= \widehat{\boldsymbol{W}}^T \varphi(\boldsymbol{z}) \end{aligned} \quad (32)$$

where $\overline{\boldsymbol{W}}$ represents the set of ideal weights, $\widehat{\boldsymbol{W}}$ represents the set of actual weights. If we define:

$$\widetilde{\boldsymbol{W}} = \overline{\boldsymbol{W}} - \widehat{\boldsymbol{W}} \quad (33)$$

the weight update law is:

$$\dot{\widetilde{\boldsymbol{W}}} = -\boldsymbol{\Gamma}\left(\varphi e^T \boldsymbol{P} - \sigma \widehat{\boldsymbol{W}}\right) \quad (34)$$

where matrix $\boldsymbol{\Gamma}$ end $\boldsymbol{P}$ define the NN learning dynamics whereas the damping term σ guarantees the weights boundedness without requiring persistent excitation.

The architecture shown in Fig. 4 has been used to augment the inner loop of the NDI control scheme (Fig. 5). A first order reference model has been used for the loop controlling rotational degrees of freedom.

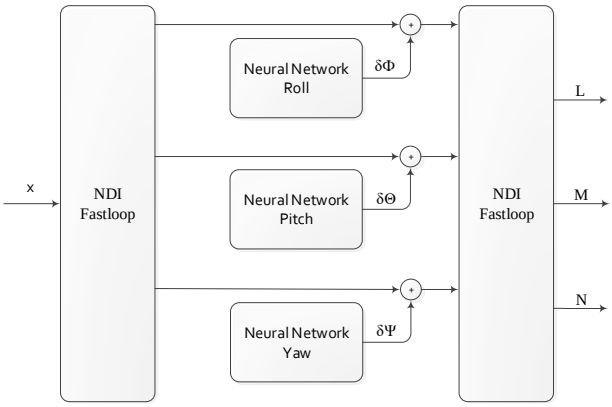

Fig. 5. NN augmented NDI fast loop

One of the major problems when implementing RBFNNs is the choice of the Gaussian basis functions parameters. In order to simplify the RBFs centers choice, a partially connected hidden layer structure has been used. According to physical considerations input parameters been selected among the most influential ones with regard the specific channels to be augmented [23].

In order to avoid a too frequent NN compensation, weights update from a specific hidden layer neuron is paused whenever RBF output is outside a given range.

Moreover, some constraints are needed to make the NN learning compatible with the embedded electronics during all the flight phases (see Fig. 6):

- Variation in the moment demand computed by NDI outside a chosen range, turns off the weight update to avoid learning during transient flight phases.
- The NN output is saturated to avoid an excessive network correction due to a constant external perturbation. Saturation stops the weight update until

the output lies in the allowable range again.

- Throttle lever must be over a certain position to avoid learning during the initial phase of take-off segment.

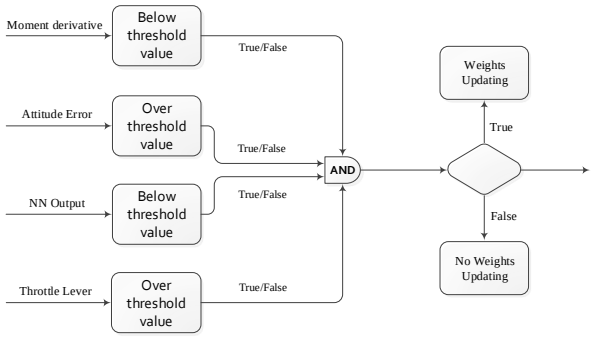

Fig. 6. NN learning diagram

5 Tri-rotor experimental setup

A Tilt-trirotor experimental flying platform has been designed and built. This mini-UAV is powered by two front (tilting) propellers and a rear (fixed) one, located at the tip of three arms joined in a circular symmetric structure (Fig. 7).

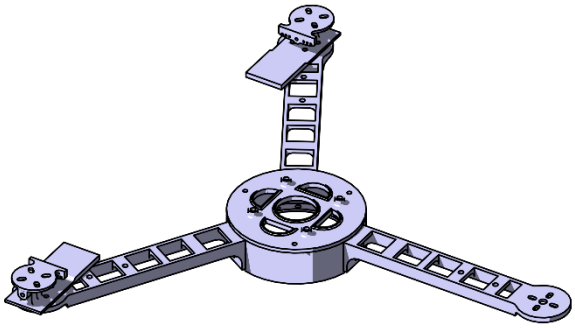

Fig. 7. Trirotor main structure

All the fixed-pitch propellers are powered by electrical brushless motors. Tilting of front propellers is provided by two position controlled angular servos. Electrical power is provided by Lithium-Polymer (Li–Po) batteries.

The FCS is based on a custom board based on a STM32F407 CPU. This board contains the Inertial Measuring Unit (including a trial axis accelerometer, a trial axis gyro, a GPS, a trial axis magnetometer and a barometer). The firmware is based on ChibiOS [24] operating system and provides the following three main tasks to CPU:

- Sensor fusion task that implements the sensor fusion algorithm, based on a Kinematic Extended Kalman Filter to provide an attitude estimation to the control system;
- Checking task of the overall system state to identify any system fault. The task is based on a state machine with four main states: initialization, idle, run and fault. Furthermore, this task analyzes also the radio system state, needed to provide reference signals to the control system;
- Control task, that implements the RBF+NDI algorithm and provides control signals to brushless motors.

6 Numerical Results and Flight Tests

6.1 Attitude Control

The effectiveness of the proposed control system was preliminarily verified by using a

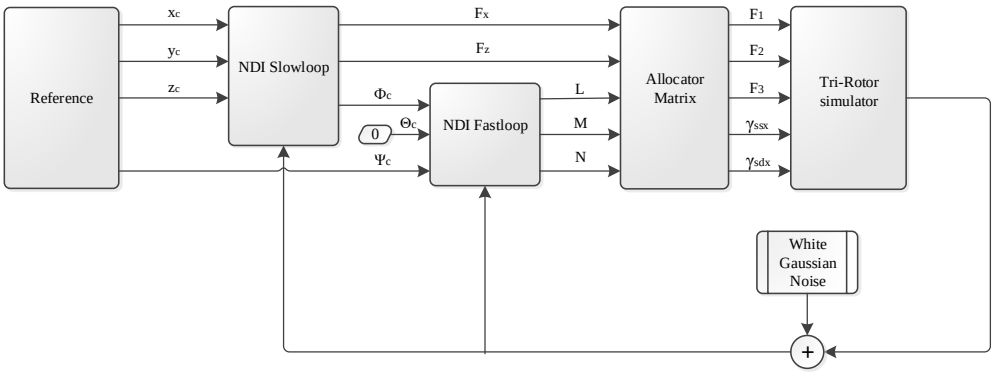

Fig. 8. Trirotor dynamics simulator

numerical simulator (Fig. 8). Tests are focused mainly to the fast loop control (i.e. attitude control system) to verify the stability and the robustness of the algorithm.

The first three maneuvers, presented in this section, are obtained using the NDI control system, without the adaptive RBF neural network.

Each simulation has been performed with the presence of external disturbances in the form of external forces and moments acting as gusts and turbulence.

As shown in Figs. 9, 10 the NDI controller is able to guarantee good results on the pitch and roll channel also without the NN augmented control.

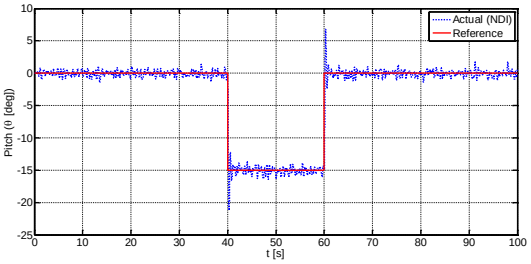

Fig. 9. Simulation results on pitch channel without NN

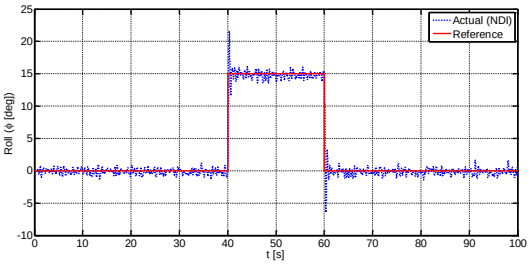

Fig. 10. Simulation results on roll channel without NN

On the other hand, less satisfactory results have been obtained on the yaw channel showing a significant offset between the reference command and the air vehicle attitude (Fig. 11). This is due to the linearization of the equations in the control allocation, resulting in a modeling error.

Therefore, whenever the system is not correctly identified most likely a steady-state error in the system response can be expected.

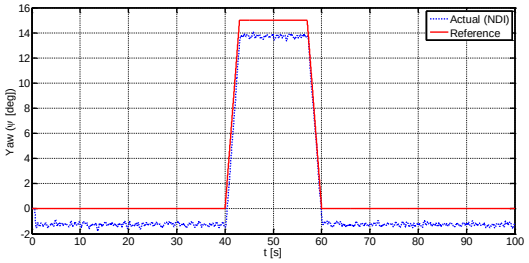

Fig. 11. Simulation results on yaw channel without NN

Further tests have been performed to test the effectiveness of the control system in the presence of non-modelled dynamics.

To this end, some usual uncertainties were introduced in the numerical simulation with regards to:

- Center of gravity position
- Inertia tensor

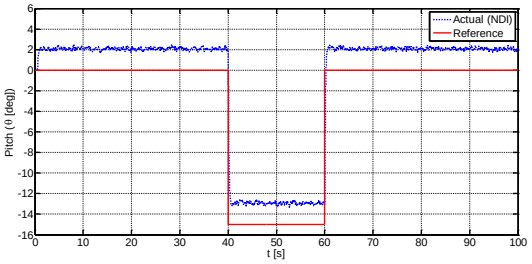

Fig. 12. Simulation results on pitch channel without NN due to 10% CG position uncertainty on x axis

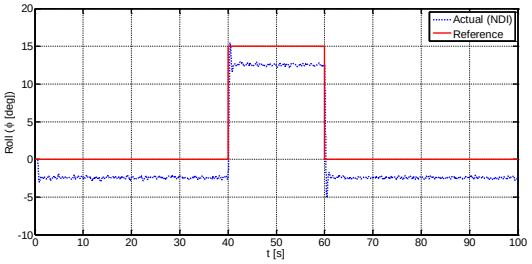

Fig. 13. Simulation results on roll channel without NN due to 10% CG position uncertainty on y axis

As we can see (Figs. 12, 13) a significant bias occurs in the system response also on pitch and roll channel as a consequence of the modelling error we have introduced. Performance of the proposed NN-augmented NDI controller are shown in Figs. 14-16.

Compared with previous results, we can see that the NN-based adaptive control system is able to reduce the steady-state error in all the cases without altering the transient dynamics of the aircraft.

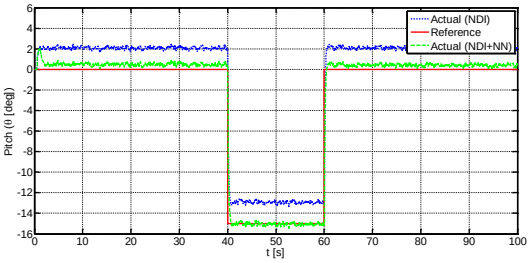

Fig. 14. Simulation results on pitch channel with and without NN due to 10% CG position uncertainty on x axis

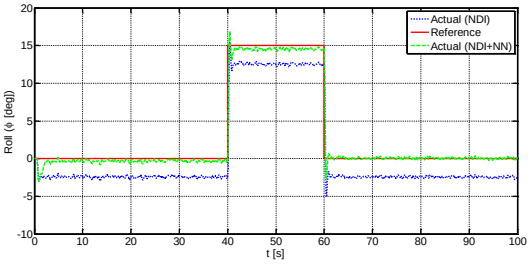

Fig. 15. Simulation results on roll channel with and without NN due to 10% CG position uncertainty on y axis

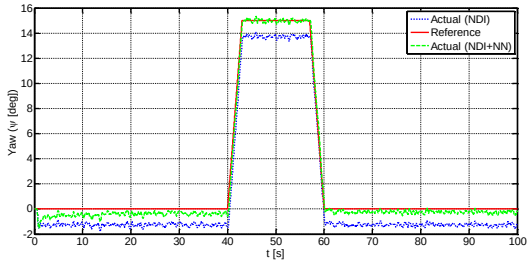

Fig. 16. Simulation results on yaw channel with and without NN

As for inertia tensor uncertainties, no significant differences have been obtained in the system response even with marked variations of vehicle inertia data (±20%). For this reason, no results have been presented in the paper.

Effectiveness of the proposed control strategy has been verified also on the tilt-trirotor experimental platform by performing several flight tests.

At first, tests were performed with the NDI control strategy without NN-based compensator. Results are shown in Figs. 17, 18.

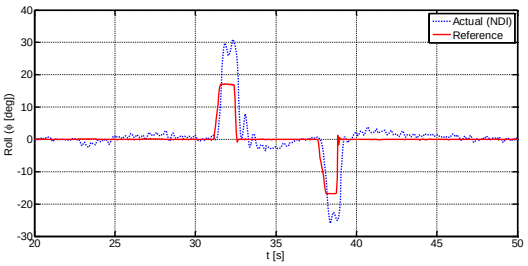

Fig. 17. Flight test results on roll channel without NN

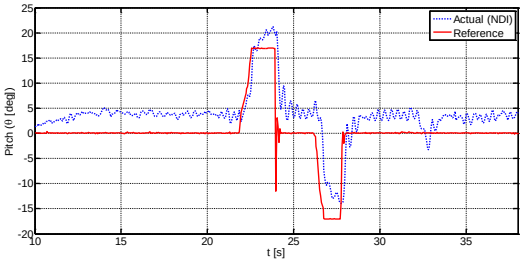

Fig. 18. Flight test results on pitch channel without NN

As we can see both on pitch and roll channel the reference command is not fully followed. In particular, as shown in Fig. 18, a significant bias results on the pitch channel as a consequence of the uncertainty about the flying platform actual CG position compared to the estimated one introduced in the model. During the flight tests campaign, this bias made the trirotor attitude more difficult to control demanding a fine trim during hovering.

Fig. 19 and Fig. 20 show flight test results with the NN-based adaptive control system.

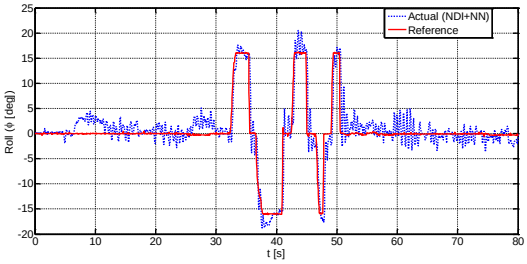

Fig. 19. Flight test results on roll channel with NN

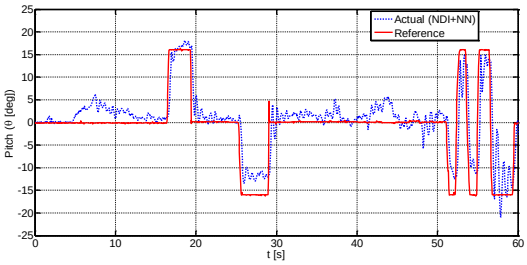

Fig. 20. Flight test results on pitch channel with NN

As we can see quite satisfactory performance of the NN-augmented control system have been obtained with a maximum error of 5 deg. This value is the maximum error allowed by the NN compensator matching the attitude estimate error due to the on-board sensors.

6.2 Trajectory Tracking Control

Finally, preliminary numerical simulations have been performed to test the effectiveness of

the slow loop control system for the trajectory tracking.

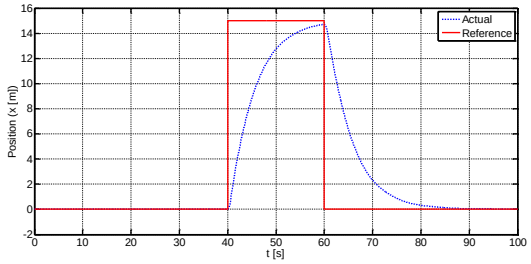

Fig. 21. Simulation results on x position channel

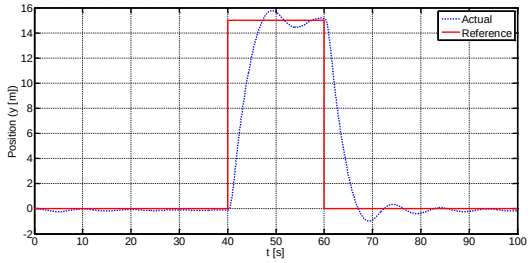

Fig. 22. Simulation results on y position channel

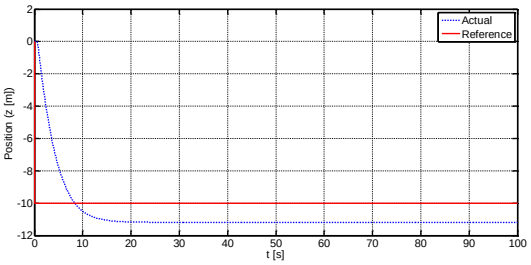

Fig. 23 Simulation results on z position channel

As we can see in Fig. 21, 22 and 23, control system allows a satisfactory trajectory tracking though different performance are obtained depending on the selected channel.

In particular, air vehicle constraint to fly at zero pitch angle and the limited tilt angle range of the front rotors needed to assure pitch control in all the flight phases lead to a quite slow maneuver on x axis (see Fig. 21).

Finally, on the z channel, the lack of an adaptive strategy (implemented only on the attitude control system) and the low accuracy in the altitude estimate by the on-board sensors lead to a clear steady-state error (Fig.23).

Conclusion

In this paper, the development of an adaptive flight control scheme based on Radial Basis Function Neural Network (RBFNN) and Nonlinear Dynamic Inversion technique (NDI) is presented. Such a control scheme has been implemented on the flight control system of a tilt-trirotor prototype model.

The effectiveness of the proposed control technique is shown by numerical simulations and experimental tests, performed by means of a scaled multi-rotor test bed.

To verify further the improvements provided by the NN-augmented control system in the presence of non-modelled dynamics, uncertainties in the center of gravity position have been introduced in the model, comparing results with and without NN compensator.

Flight tests were successfully carried out showing good performance of the novel attitude control system also in the presence of external disturbances.

As for trajectory tracking the proposed control strategy was tested only by means of numerical simulations. Currently, we are working on the setup of a flight arena to test indoor trajectory tracking capabilities. Dedicated flight tests are planned for the near future.

References

[1] F. Çakici e M. K. Leblebicioglu, «Analysis of a UAV that can Hover and Fly Level,» in *MATEC Web of Conferences*, 2016.

[2] M. D. Maisel, D. J. Giulianetti e D. C. Dugan, «The history of the XV-15 tilt rotor research aircraft from concept to flight,» 2000.

[3] T. R. Quackenbush, J. D. Keller e G. R. Whitehouse, «Analysis Methods for Advanced V/STOL Configurations,» in *AHS 72nd Annual Forum, West Palm Beach, Florida, May 17–19*, 2016.

[4] Y. Kang, B. Park, C. Yoo, Y. Kim e S. Koo, «Flight test results of automatic tilt control for small scaled tilt rotor aircraft,» in *Control, Automation and Systems, 2008. ICCAS 2008. International Conference on*, 2008.

[5] Y.-s. Kang, B.-j. Park, A. Cho, C.-s. Yoo e S.-O. Koo, «Flight test of flight control performance for airplane mode of Smart UAV,» in *Control, Automation and Systems (ICCAS), 2012 12th International Conference on*, 2012.

[6] D. A. Ta, I. Fantoni e R. Lozano, «Modeling and control of a tilt tri-rotor airplane,» in *American Control Conference*, 2012.

[7] A. B. Chowdhury, A. Kulhare e G. Raina, «Back-

stepping control strategy for stabilization of a tilt-rotor uav,» in *Control and Decision Conference (CCDC), 2012 24th Chinese*, 2012.

[8] C. Yu, J. Zhu, J. Hu e Z. Sun, «Experimental modeling using modified cascade correlation RBF networks for a four DOF tilt rotor aircraft platform,» *Neurocomputing*, vol. 69, n. 13, pp. 1802-1805, 2006.

[9] N. Amiri, A. Ramirez-Serrano e B. Davies, «Nonlinear adaptive control of a new configuration of rotary wing unmanned aerial vehicle,» in *Electrical \& Computer Engineering (CCECE), 2012 25th IEEE Canadian Conference on*, 2012.

[10] Z. Chen, C. Yu e J. Yang, «Dynamic modeling using cascade-correlation RBF networks for tilt rotor aircraft platform,» in *Neural Networks and Brain, 2005. ICNN\&B'05. International Conference on*, 2005.

[11] L. Wang, Y. He, Z. Zhang e C. He, «Trajectory tracking of quadrotor aerial robot using improved dynamic inversion method,» *Intelligent Control and Automation*, vol. 4, n. 04, p. 343, 2013.

[12] R. Rysdyk, F. Nardi e A. J. Calise, «Robust adaptive nonlinear flight control applications using neural networks,» in *American Control Conference, 1999. Proceedings of the 1999*, 1999.

[13] S. Sieberling, Q. P. Chu e J. A. Mulder, «Robust flight control using incremental nonlinear dynamic inversion and angular acceleration prediction,» *Journal of guidance, control, and dynamics*, vol. 33, n. 6, pp. 1732-1742, 2010.

[14] G. Di Francesco, E. D'Amato e M. Mattei, «Incremental Nonlinear Dynamic Inversion and Control Allocation for a Tilt Rotor UAV,» in *Guidance Navigation and Control Conference Proceedings, AIAA Scitech*, 2014.

[15] R. T. Rysdyk e A. J. Calise, «Adaptive model inversion flight control for tilt-rotor aircraft,» *Journal of Guidance, Control, and Dynamics*, vol. 22, n. 3, pp. 402-407, 1999.

[16] E. Johnson, A. J. Calise, H. A. El-Shirbiny e R. T. Rysdyk, «Feedback linearization with neural network augmentation applied to X-33 attitude control,» in *Proceedings of the AIAA Guidance, Navigation, and Control Conference*, 2000.

[17] M. Idan, M. Johnson e A. J. Calise, «Hierarchical approach to adaptive control for improved flight safety,» *Journal of guidance, control, and dynamics*, vol. 25, n. 6, pp. 1012-1020, 2002.

[18] G. Chowdhary, J. How e H. Kingravi, «Model reference adaptive control using nonparametric adaptive elements,» in *Conference on Guidance Navigation and Control, Minneapolis, MN*, 2012.

[19] R. Rysdyk e A. J. Calise, «Robust nonlinear adaptive flight control for consistent handling qualities,» *Control Systems Technology, IEEE Transactions on*, vol. 13, n. 6, pp. 896-910, 2005.

[20] D.-W. Yoo, H.-D. Oh, D.-Y. Won e M.-J. Tahk, «Dynamic modeling and stabilization techniques for tri-rotor unmanned aerial vehicles,» *International Journal of Aeronautical and Space Sciences*, vol. 11, n. 3, pp. 167-174, 2010.

[21] S. Salazar-Cruz, R. Lozano e J. Escare{\~n}o, «Stabilization and nonlinear control for a novel trirotor mini-aircraft,» *Control Engineering Practice*, vol. 17, n. 8, pp. 886-894, 2009.

[22] J. Escareno, A. Sanchez, O. Garcia e R. Lozano, «Triple tilting rotor mini-UAV: Modeling and embedded control of the attitude,» in *American Control Conference, 2008*, 2008.

[23] E. D'Amato, G. Di Francesco, I. Notaro, G. Tartaglione e M. Mattei, «Nonlinear Dynamic Inversion and Neural Networks for a Tilt Tri-Rotor UAV,» *IFAC-PapersOnLine*, vol. 48, n. 9, pp. 162-167, 2015.

[24] G. Di Francesco, «Nonlinear Control of a Tilt Rotor UAV,» 2014.

[25] G. D. Sirio, «www.chibios.org,» [Online].

Copyright Statement